JREE: Vol. 9, No. 4, (Autumn 2022) 109-121

Journal of Renewable Energy and Environment

Journal Homepage: www.jree.ir

Materials and Energy Research Center

MERC

Research Article

Multiobjective Design Optimization of a Multi-Phase Outer-Rotor Permanent Magnet Wind Generator

Ali Ebadi *, Ali Akbar Abdoos, Mohammad Ebrahim Moazzen, Sayyed Asghar Gholamian

Department of Electrical and Computer Engineering, Babol Noshiravani University of Technology, P. O. Box: 47148-71167, Babol, Mazandaran, Iran.

PAPER INFO

Paper history:
Received: 28 February 2022
Revised in revised form: 02 June 2022
Scientific Accepted: 20 June 2022
Published: 18 December 2022

Keywords:
Optimization,
Permanent Magnet Generator,
Wind Power,
Genetic Algorithm

ABSTRACT

Nowadays, the Permanent Magnet (PM) generator has become an instrumental tool for wind power generation due to its high performance. In this study, an optimal design is established to provide a cost-effective multiphase outer-rotor PM wind generator (OR-PMWG). The cost of the generation system (generator and power converter) as well as the annual energy output must be optimized to ensure cost-effective PM wind generation. In fact, the main novelty of this paper lies in the presentation of an accurate model of OR-PMWG and the investigation of the design variables affecting annual energy output and the generation system cost (GSC). In this respect, a multi-objective framework is presented to make satisfactory agreement among all objectives. At first, the main optimal design objectives namely generation system cost and annual energy output are optimized separately and then, a multi-objective optimization is established, in which all the objectives are considered simultaneously. In order to tackle these optimization problems, Genetic Algorithm (GA) is adopted herein to determine the design variables. It is also shown that simultaneous optimization with 71.39 (MWh) AEO and 2651.51 (US$) GSC leads to a more optimal design for a PM wind generation system. In addition, the effectiveness of the presented optimal design is demonstrated by making a comparison between a prototype outer-rotor PM wind generator and the theoretical counterpart. Finally, a finite element analysis (FEA) is carried out for the validation of the outcomes obtained from the proposed optimal design.

https://doi.org/10.30501/jree.2022.317176.1287

1. INTRODUCTION

In recent years, due to the precipitous depletion of fossil fuels, increased energy costs, and environmental issues, the demand for a reliable and sustainable alternate source of energy has been highlighted. Potentially, renewable energy resources are becoming more viable technology to resolve this concern. Among renewable resources, wind energy generation has exhibited dramatic development, which can be attributed to infinite resources, low production cost, and environmentally-friendliness. Moreover, in comparison with other renewable resources, the scope of wind power market is growing substantially [1, 2]. In fact, the global-scale installed capacity of wind power has grown swiftly during the past two decades, from 18 GW in 2000 to 743 GW at the end of 2019 [3]. There is an increasing interest in the development of a small-scale wind power system because large-scale wind farms do not represent a sustainable alternative for renewable power generation. Therefore, the best available option is the installation of decentralized wind power systems that comprise small-scale wind farms. The unit installation costs and the expenses for production per power unit for small-scale wind power generation, among other wind power generation systems, are smaller than those for solar power generation with the same capacity [4]. Generally, a wind turbine according to the construction of drive trains can be classified into direct-drive and geared-drive concepts. Low maintenance, high efficiency, energy efficiency, and reliability requirements for wind power generation tend to use gearless concept [5, 6]. Furthermore, among different types of electrical generators available for converting the wind power, the permanent magnet synchrounes generator (PMSG) has huge potential for this application because of its higher efficiency, torque density, reliability, and lower maintenance [6, 7]. Polinder et al. [8] compared different well-known types of employable generator systems for wind turbines in view of annual energy output and cost for a given wind climate. They concluded that the direct-drive PM wind generator (DD-PMWG) was the best choice on account of the above-mentioned advantages as well as the elimination of brushes or gearbox. This machine can be divided into two categories from the viewpoint of the rotor-stator structure including inner and outer rotor types, in which the second one has a better performance in terms of cooling and saturatio [9].

Based on the above descriptions, designing high-performance PM generators and wind turbines optimally has become more important day by day. In [10], the Lagrange

*Corresponding Author's Email: ebadi.power@gmail.com (A. Ebadi)
URL: http://www.jree.ir/article_155019.html

Please cite this article as: Ebadi, A., Abdoos, A.A., Moazzen, M.E. and Gholamian, S.A., "Multiobjective design optimization of a multi-phase outer-rotor permanent magnet wind generator", ***Journal of Renewable Energy and Environment (JREE)***, Vol. 9, No. 4, (2022), 109-121. (https://doi.org/10.30501/jree.2022.317176.1287).

multiplier as a simple analytical optimization method was employed to maximize the air-gap apparent power of the PMSG under tangential stress constraint. A combination of the simple magnetic equivalent circuit approach and the finite-element method was established in [11] to achieve an optimum design of an outer-rotor PM wind generator using a high-energy neodymium-iron-boron magnet. Based on the results of an optimal design presented by Li et al. [12], the multi-bird concept of PM generator was more cost-effective than the direct-drive one. The cogging torque and total harmonic distortion (THD) of back electromotive force of the small-scale outer-rotor PM wind generator were minimized by a multi-objective optimization design method proposed by Lee et al. [13]. Bazzo et al. [14] presented a multi-physics design of a PM generator so that the cost and losses of the grid side power electronic converters could be taken into account. In [15], the optimization of the direct drive PM generators was accomplished to reduce the cost of energy in offshore wind turbines. Asef et al. combined the modified Booth's algorithm and a dual-response surface method for the purpose of multi-objective design optimization of a PMSG [16]. The output power maximization and manufacturing cost minimization were considered as two main objectives to improve the performance of power generation under a number of design constraints. In some papers, the main focus of design optimization of PM wind generators is to reduce the cogging torque [17, 18]. In [19], a compact BEM (blade element momentum) analysis was derived to design optimal blades for continuously variable speed horizontal axis wind turbines. The present BEM modeling may be useful to reduce the computational effort of iterative numerical methods used in determining off-design power performance of conventional wind turbines with constant speed. In [20], the circulating aerofoil for use in Magnus-type wind turbine was introduced which utilized the treadmill motion in a simple and easy manner to manufacture aerofoil surfaces. It is proved here that the concept of generating Magnus lift from circulating aerofoil surface is computationally valid. In [21], artificial neural network (ANN) modeling was employed to investigate the effects of various environmental and machine factors on the energy gain from wind farm systems. It was demonstrated that ANN was a better statistical predictor based on numerical comparison with non-linear regression. Since the gearless wind generators operate at relatively low speeds, they are known by their large dimensions, volume, and heavy weight. In practical applications, low system cost and high annual output energy are two main advantages for a cost-effective wind power system.

In this paper, a multi-objective framework is oriented to minimize the cost of generation system and to maximize annual the output energy of the generation system. The global cost of a wind power system includes the costs of production, transportation, and installation of all components, like electrical generator, power electronic converter, and turbine blades and tower. Also, the operational as well as maintenance costs of the system should be calculated [22]. The calculation of these costs is difficult and is often estimated by adopting several assumptions. Hence, this research only considers the PM generator and power converter costs. The six-phase PM wind generator is proposed to increase the reliability of the wind power generation. It is noteworthy to mention that this type of generator can continue operating during faults using the remaining healthy phases. Reducing the torque pulsation amplitude and reducing the current phase amplitude of armature without increasing the phase voltage are the other advantages of multiphase machines [23]. In this study, the six phases of the generator are arranged as a two-star configuration. For more reliability, each three-phase set is supplied by a back-to-back power converter and the converters are connected as parallel. Figure 1 indicates a schematic view of the grid-connected DDPMWG.

This paper is organized as follows. In Section 2, the modeling of the OR-PMWG concept is described. The design variables are presented in Section 3. Optimal design results are presented in Section 4, and also the results are compared with a prototype. Then, the design validity is verified by 3D finite element analysis in Section 5. Finally, conclusions are given in Section 6.

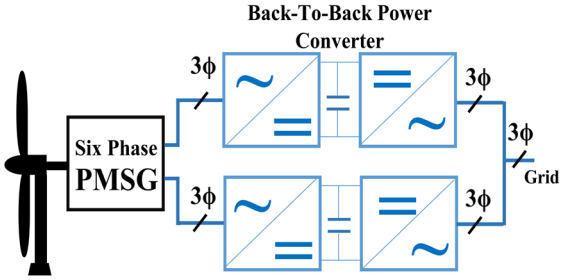

Figure 1. Configuration of the multiphase DD-PMWG system

2. MODELING THE OR-PMWG CONCEPTS

The generator specifications and explanation of its structure are described at the beginning of this section. Thereafter, geometrical relationships of the generator are outlined. The calculation of the generator losses and OR-PMWG costs comes after that. Next, the wind turbine modeling and annual energy output calculation in this case study are described. Finally, the overview of the design model is presented as a flowchart.

2.1. PMSG specifications

There are various types of PM machines that can be employed in the low-speed, gearless large wind turbines. However, because of high torque density, simple structure, and suitable reliability, the radial-flux concept with surface-mounted PMs can be counted as a better option [5, 22]. Generally, there are two configurations of the radial-flux PMSG: inner outer rotor types. In the case of the outer rotor structure, the outer part is rotor, and the stator is inside of machine, as shown in Figure 2a. Figure 2b illustrates the main geometrical parameters of a radial-flux, surface-mounted outer-rotor PMSG (OR-PMSG). The inner rotor type is mostly used, whereas the outer rotor structure is having few applications. However, in order to cope with the various difficulties in designing a DD-PMWG, the outer rotor configuration was adopted in this paper. Following are the several advantages of OR-PMSG [7, 9, 11, 13]:

(a) The hub of the turbine blades can be conveniently fixed to the exterior rotor; therefore, this structure can be well adapted to wind power application.

(b) Unlike the inner rotor type, the cooling condition for the PMs is improved, because the outer rotor is directly exposed to the wind.

(c) Regarding the large rotor diameter, multi-pole magnets can be applied in order to generate power at low speeds.

(d) The multi-pole structure leads to (1) the reduction of the total length of the magnetic flux path and a noticeable decrease in the volume and weight of the rotor back iron and (2) shorter coil pitch and resulting end-winding than the inner rotor. Therefore, the copper loss is lower.

The six-phase stator winding is divided into two star-connection and three-phase sets, i.e., winding sets of ABC and XYZ (see Figure 3). According to this figure, the proposed generator has symmetrical 60° displacement windings. It should be noted that the neutral points of the two star-connection winding sets are considered not to be connected together. By doing so, a winding becomes immune to physical fault events on the other winding, leading to higher reliability. Consequently, the flow of triplen harmonics in line-to-line voltage is prevented [24]. Specific parameters of OR-PMSG are listed in Table 1. The following assumptions are made in the OR-PMSG design optimization:

(1) In order to provide an almost sinusoidal induced voltage, the stator winding is a two-layer distributed winding. Moreover, to minimize both the 5th and 7th time harmonics, the coil span is equal to 5/6 of the pole pitch.

(2) The air-gap is one thousandth of the outer diameter of stator [6, 25].

(3) The NdFeB35 is selected as PM material with remanent flux density B_r = 1.23 T.

(4) Since the PM wind generator is connected to grid via power electronic converter, it is assumed that the PMSG runs at the unity power factor and at all wind speeds [26].

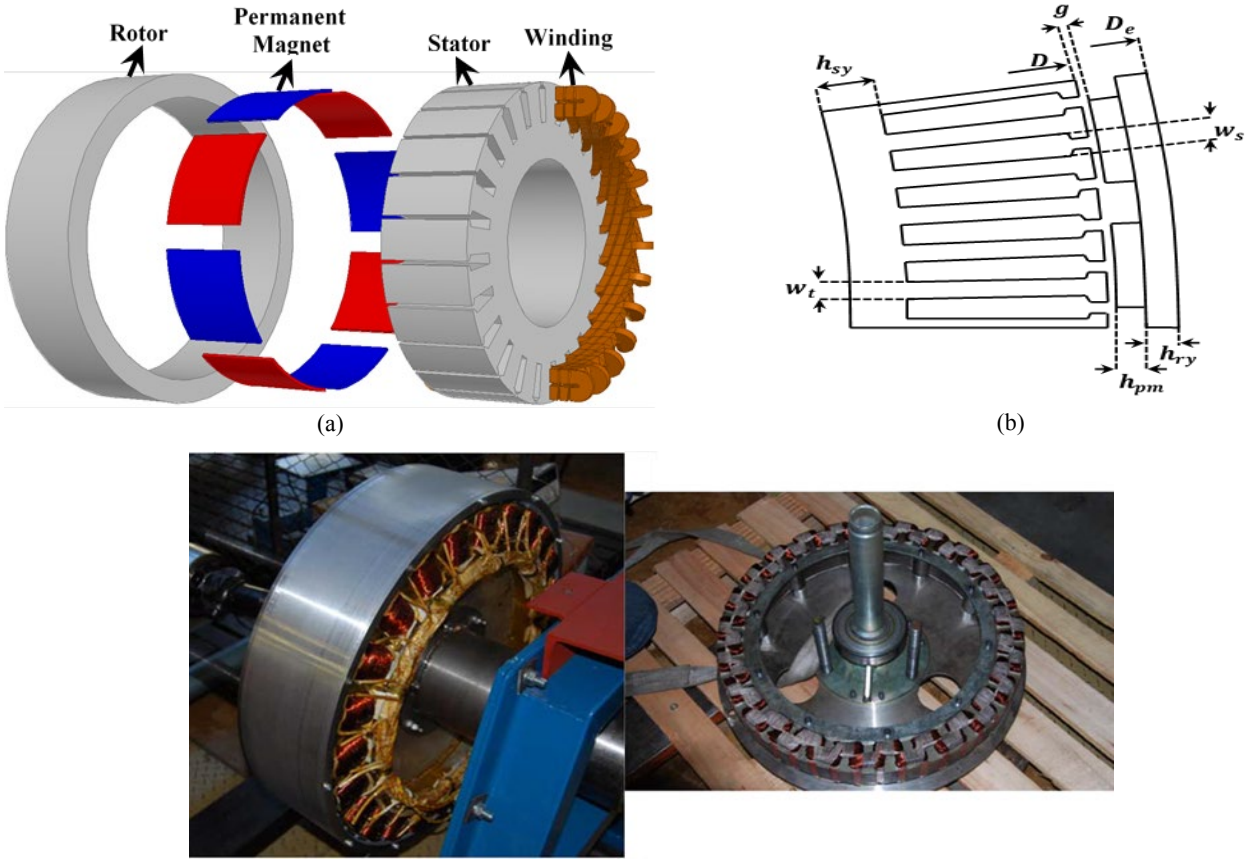

Figure 2. (a) Radial-flux PM machine construction with outer rotor, (b) Typical cross section of the OR-PMSG, (c) The real configuration of OR-PMSG [17]

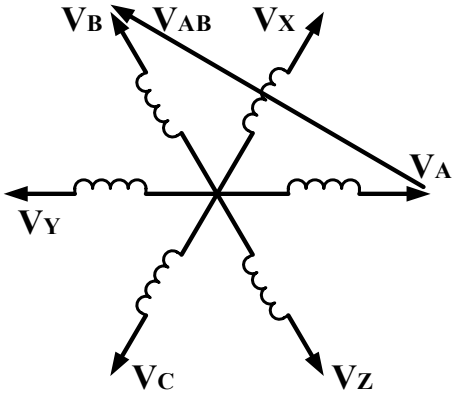

Figure 3. Phasor diagram of the six-phase winding connections

Table 1. Modeling constants and generator main parameters

Parameters and constants	Value
Main design parameters	
Nominal output power (W)	15000
Nominal Line voltage (V)	400
Nominal shaft speed (rpm)	150
Number of slots per pole per phase	2
Current density (A/mm^2)	5
Iron core specifications	
ρ_h (W/kg)	2
ρ_e (W/kg)	0.5
Cost modeling constants	
Copper cost (US$/kg)	9.61
Permanent magnet cost (US$/kg)	220.31
Iron core cost (US$/kg)	2.62
Reference structure cost (US$)	3250

2.2. Generator geometrical modeling

In this subsection, the analytical models are established to calculate various dimensions of the generator. To extract an analytic relationship between the geometric dimensions and magnetic parameters, the air-gap apparent power is developed in terms of the current and induced voltages of the stator winding. The induced voltage by air-gap flux density can be presented as follows:

$$e(t) = \sqrt{2}\, E_{rms} \sin(2\pi ft) \quad (1)$$

where f is frequency. The rms value of the induced voltage E_{rms} as a function of the generator dimensions can be calculated as follows [8, 12]:

$$E_{rms} = \frac{\sqrt{2}}{2} N_{ph} \omega_m D L B_{mg1} k_{w1} \quad (2)$$

wherein N_{ph}, ω_m, and k_{w1} are the winding turns per phase, the mechanical angular speed of the rotor, and fundamental winding factor, respectively. Also, L and D are the machine length and stator outer diameter, respectively, and B_{mg1} is the highest fundament harmonic value of the air-gap flux density due to the PMs, which is obtained as follows [8, 27]:

$$B_{mg1} = \frac{4}{\pi} B_{mg} \sin\left(\frac{\pi}{2}\alpha_i\right) \quad (3)$$

where the air-gap flux density peak value B_{mg} and the pole-arc to pole-pitch ratio α_i are illustrated in Figure 4. B_{mg} in PM machines depends on the PM material properties and allowable flux density in the machine teeth. To reduce the amount of needed copper as well as the volume and weight of the machine, the magnetic air gap flux density for low- and medium-speed applications must be high enough. Because of its high residual flux density and energy generation, the NdFeB magnet is technically the best choice for this machine [28]. Therefore, for the sizing procedure of PM machine using NdFeB, the value of the air-gap flux density peak is initially chosen to be 60-80 % for Br [27]. The range of values for α_i as one of the design variables is chosen to be 0.6-0.9 [6]. By introducing the peak value expression of stator linear current density, A_m, the current waveform rms value is as follows [10, 12]:

$$I_{rms} = \frac{\pi D A_m}{2m\sqrt{2}\, N_{ph}} \quad (4)$$

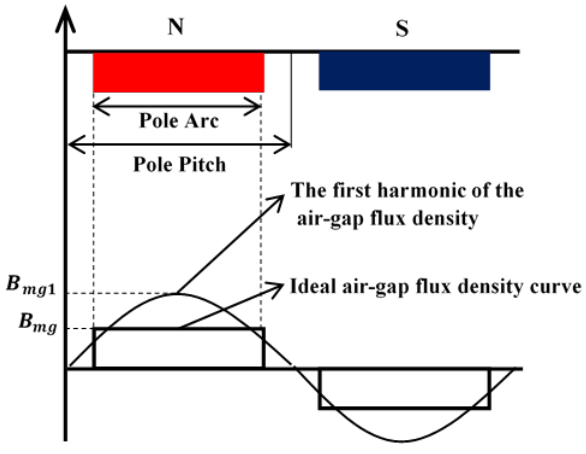

Figure 4. The ideal curve of the air-gap magnetic flux density distribution above the magnets in an electric period

where m stands for the number of phases. The specific electric loading is determined based on the machine cooling system and efficiency [28]. The amplitude of the specific electric loading ranges from 10000 to 55000 A/m for medium power machines [27]. Therefore, the current expression takes the following form:

$$i(t) = \sqrt{2} I_{rms} \sin(2\pi ft) \quad (5)$$

The average apparent power crossing the air-gap over one period of the power source can be expressed as:

$$S_g = \frac{m}{T}\int_0^T e(t).i(t)\, dt \quad (6)$$

By substituting Eqs. (1) and (5) into Eq. (6), the air-gap apparent power in terms of the generator main dimensions can be written as follows:

$$S_g = 0.5\pi^2 k_{w1} n_s D^2 L A_m B_{mg1} \quad (7)$$

where n_s is the rotational speed of the rotor in rev/sec. (since). Then, the output power is calculated as follows:

$$P_{out} = \frac{1}{\epsilon} S_g \cos(\phi) \quad (8)$$

The generator main dimensions in terms of the output power can be expressed as follows:

$$D^2 L = \frac{P_{out}.\epsilon}{0.5\pi^2 A_m B_{mg1} n_s k_{w1} \cos(\phi)} \quad (9)$$

In which P_{out} denotes the nominal output power of the PMSG. ϵ is the ratio of the induced voltage to the full load terminal voltage. In addition, $\cos(\phi)$ stands for the load power factor. In the electrical machine design, the relative apportionment of the machine length and air-gap diameter depends on its application. For the direct-drive radial-flux PM wind generator, the suitable range for the ratio of the generator length to air-gap diameter is 0.14-0.5 [29]. Based on Ampere's circuital law, the BH characteristic of a PM material, magnetic flux continuity, and geometry are shown in Figure 2 and the PM height as a function of magnetic air-gap flux density can be expressed as [6, 12]:

$$h_{pm} = \frac{B_{mg}}{B_r} \mu_{rec} g_{eff} \quad (10)$$

where g_{eff} is the effective air-gap length and μ_{rec} is the PM recoil line relative permeability. The stator teeth, rotor, and stator yoke provide the return paths for flux between poles. Therefore, dimensions of these parts are calculated by the allowed magnetic flux densities. The stator tooth width w_t, rotor, and stator yoke height h_y can be presented by [6, 30]:

$$w_t = \frac{\pi D}{k_{st} Q} . \frac{B_{mg}}{B_t} \quad (11)$$

$$h_y = \frac{D}{k_{st} P} . \frac{B_{mg}}{B_y} \quad (12)$$

where k_{st}, Q, and P denote the stacking factor for the stator core, number of slots, and poles, respectively. Also, B_t and B_y are the maximum tooth and yoke flux density, respectively.

2.3. OR-PMWG losses modeling

The considered losses in this study are the basic losses of the OR-PMWG, i.e., the stator iron losses P_{Fe}, the generator copper losses P_{Cu}, and the back-to-back power converter losses P_{BPC}. In fact, the generator total losses are the sum of P_{Fe} and P_{Cu}. Also, the sum of these losses with power converter losses is called total generation loss. The rotor iron losses are negligible in the surface-mounted PM machine due to their large effective air-gap [27]. The mechanical losses in the electrical machines consist of friction in couplings and bearings and windage losses. Here, the mechanical losses will not be considered because they are usually small [31]. Therefore, the total generation losses are determined as follows:

$$P_{loss} = P_{Fe} + P_{Cu} + P_{BPC} \quad (13)$$

The iron losses can be calculated approximately using Steinmetz formula as follows [8, 15]:

$$P_{Fe} = 2m_{Fe}\rho_h \frac{f}{50}\left(\frac{B_{Fe}}{1.5}\right)^2 + 2m_{Fe}\rho_e \left(\frac{f}{50}\right)^2 \left(\frac{B_{Fe}}{1.5}\right)^2 \quad (14)$$

where f, B_{Fe}, and m_{Fe} are the frequency of the field in the iron, stator teeth or yoke flux density, and iron weight, respectively. ρ_e is the specific eddy current loss and ρ_h is the specific hysteresis loss w/kg at flux density 1.5 T and frequency 50 Hz [8, 16]. For the calculation of total iron losses, the hysteresis and eddy current losses in various parts (teeth and yokes) are determined and then added. The iron core specifications are given in Table 1. The peak magnetic flux densities in the teeth and stator and rotor yoke are of the most important limitations in designing an electrical machine and also chosen as design variables. The copper losses are given by:

$$P_{Cu} = mR_s {I_{rms}}^2 \quad (15)$$

Various ways to estimate the power converter losses are presented. In this study, the losses of each three-phase back-to-back power converter are calculated as [5, 8]:

$$P_{BPC} = \frac{P_{CN}}{31}\left(1 + 10\frac{I_P}{I_{PN}} + 5\left(\frac{I_P}{I_{PN}}\right)^2 + 10\frac{I_G}{I_{GN}} + 5\left(\frac{I_G}{I_{GN}}\right)^2\right) \quad (16)$$

where P_{CN} denotes the converter loss at the nominal power which is 3 % of it, I_P denotes the PMSG side current, and I_{PN} is the PMSG side converter nominal current. I_G and I_{GN} are the grid side current and nominal current of the grid side converter, respectively.

2.4. OR-PMWG cost modeling

The proposed model considers the generator cost and costs of power electronic converters to estimate the cost of a generation system. The OR-PMWG cost C_{OP} can be calculated by summing up the active material and generator structure costs. The cost of the back-to-back power converter (BPC) for different power ratings includes OR-PMWG side power converter (OSPC), grid side power converter (GSPC), capacitors, drivers, protections, and heat-sink system [14]. The cost of active materials (C_{act}) based on the relevant specific cost (c_{Cu}, c_{PM}, and c_{Fe}) can be expressed by the sum of the copper, PM, and core weights (w_{Cu}, w_{PM}, and w_{Fe}) in the following:

$$C_{act} = w_{PM}c_{PM} + w_{Cu}c_{Cu} + w_{Fe}c_{Fe} \quad (17)$$

Furthermore, an approximate model is used for the structure cost C_{str}; thereafter, it is calculated based on the rotor outer diameter D_e and length of the generator as follows [6, 19]:

$$C_{st} = \frac{c_{str}}{2}\left[\left(\frac{D_e}{D_{ref}}\right)^a + \left(\frac{L}{L_{ref}}\right)^a\right] \quad (18)$$

where c_{str} denotes a reference machine specific cost with the diameter (D_{ref}) of 1.0 m and the length (L_{ref}) of 0.3 m. The exponent a (set to 3) describes how fast the structure cost increases with increasing rotor outer diameter and length of generator. The BPC cost of each three-phase power converter is calculated as follows [14]:

$$C_{BPC} = 725.\, e^{0.0145\, I_{rms}} \quad (19)$$

Finally, the total cost that is obtained by summing up the OR-PMSG and the BPC costs can be written as follows:

$$C_t = C_{OP} + C_{BPC} \quad (20)$$

Table 1 presents the costs of different components.

2.5. Modeling of wind turbine

The wind turbine shaft speed as a function of wind speed, available nominal power on the shaft, and annual energy output (AEO) of generation systems should be calculated using this sub-model. In this paper, the wind turbine with a horizontal axis is used and it enjoys a number of advantages over vertical axis type including higher aerodynamic efficiency and higher tip-speed ratio.

2.5.1. Power absorption and shaft speed

The nominal speed of the OR-PMSG, which has direct impact on the overall size, can be estimated from the wind energy equations. The wind turbine absorbs power P_T as a function of the wind speed v and it can be calculated as follows [14, 32, 33]:

$$P_T = 0.5C_p\rho_{air}\pi R^2 v^3 \quad (21)$$

where ρ_{air} is the air density and R is the radius of the turbine blade. C_p is the aerodynamic efficiency with typical values between 0.3 and 0.45, which is a function of the tip speed ratio λ. Furthermore, λ can be expressed as [32, 33]:

$$\lambda = \frac{\omega_r R}{v} \quad (22)$$

wherein $\omega_r = 2\pi n_r/60$ is the angular shaft speed rad/s and n_r denotes the rotational speed rpm. The range of the values for the tip-speed ratio is 6-8 [1], or 5-7 [22]. Finally, by combining Eqs. (21) and (22), one can obtain an estimation of the operating shaft speed as a function of the generator output power [29, 32]:

$$\omega_r = \sqrt{\frac{0.5C_p\rho_{air}\pi\lambda^2 v^5\eta_g}{P_{out}}} \quad (23)$$

where η_g is the efficiency of the generator, which is assumed to be 0.9 for shaft speed estimation [5]. The wind speed is one

of the important input parameters for the calculation of the nominal shaft speed. In this study, its range is considered 5-10.2 m/s. It should be noted that this range of wind speeds has been reported for Hamoon region in Iran [33]. Therefore, OR-PMSG is designed to operate at a wind speed of 10 m/s. The characteristics of the wind turbine as well as the wind site are summarized in Table 2. Assuming a 10 m/s wind speed and using the characteristics given in Table 2, the nominal shaft speed can be estimated at 150 rpm or 2.5 rev/s. The small-scale PM wind generators frequency has a normal range that is reported to be 10-70 Hz [29] or 30-80 Hz [11]. Thus, for the purpose of this paper, the generator pole number as an optimization variable varies from 8 to 64.

2.5.2. Annual energy output calculation

To assess the economic feasibility of the wind turbine installation at a specific site, the estimation of the annual output energy is very important. The AEO estimation depends on many parameters, e.g., average wind speed and operational and power characteristics of the wind turbine. The operating and power characteristics of the wind turbines at different wind speeds can be described conventionally as a power curve, which is shown in Figure 5. It has three zones based on the velocity scale [2, 19]:

Zone A: The power extracted from the wind turbine is zero, because the wind is very light for useful energy production.

Zone B: The lower limit of this zone is the cut-in wind speed v_i. The wind turbine commences power production Above v_i. In this zone, the control system of the wind turbine to capture the maximum wind power regulates the shaft speed for each wind speed.

Zone C: In this zone, the wind speeds are above nominal value v_r. The rotational speed and power are kept constant Above v_r, and the maximum power output of the electrical generator is obtained. Beyond the cut-out wind speed v_o, the wind turbine shuts off.

By integrating the product of the probability density function $f(v_j)$ of wind speed with the generation system output power, the AEO of the generation system (generator and power converter) can be approximately estimated as follows [12]:

$$AEO_G = 24 \times 365 \int_{v_i}^{v_o} \eta_{gs}(v).P_T(v).f(v)dv = 8760 \sum_{j=1}^{n} \eta_{gs}(v_j).P_T(v_j).f(v_j)\Delta v \quad (24)$$

where η_{gs} is the efficiency of the generation system. The wind data can be well fitted into the Rayleigh distribution function. The expression of Rayleigh distribution function, which describes the probability of having a wind speed during the year, is expressed as follows [31, 31]:

$$f(v_j) = \frac{\pi}{2}\frac{v_j}{(\bar{v})^2} e^{-\frac{\pi}{4}(\frac{v_j}{\bar{v}})^2} \quad (25)$$

where v_j is the particular wind speed and $\bar{v}$ is the average wind speed.

Table 2. Wind turbine and wind site specifications

Specifications	Value
Nominal wind speed (m/s)	10
Average wind speed (m/s)	8.7
Cut-in wind speed (m/s)	4
Cut-out wind speed (m/s)	25
Nominal turbine shaft speed (rpm)	150
C_p	0.42
λ	7

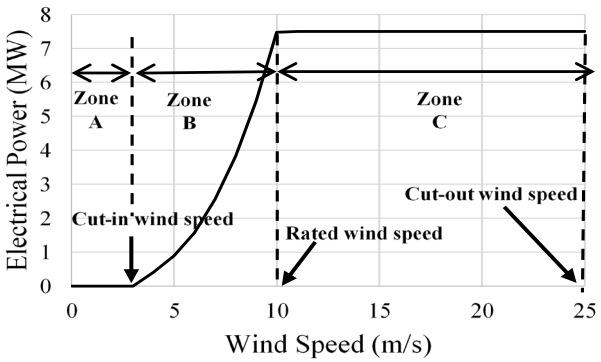

Figure 5. Operational zones of a wind power generation

2.6. Design flow chart

Figure 6 shows the proposed design procedure. As introduced earlier, the design variables are determined by the GA to achieve the minimal generation system cost and maximum AEO. Afterwards, different generator parameters are calculated. Accordingly, the magnetic air gap flux density and the terminal voltage at nominal load are computed. If one of the termination criteria is satisfied, the optimization procedure stops; if else, it will cease to operate.

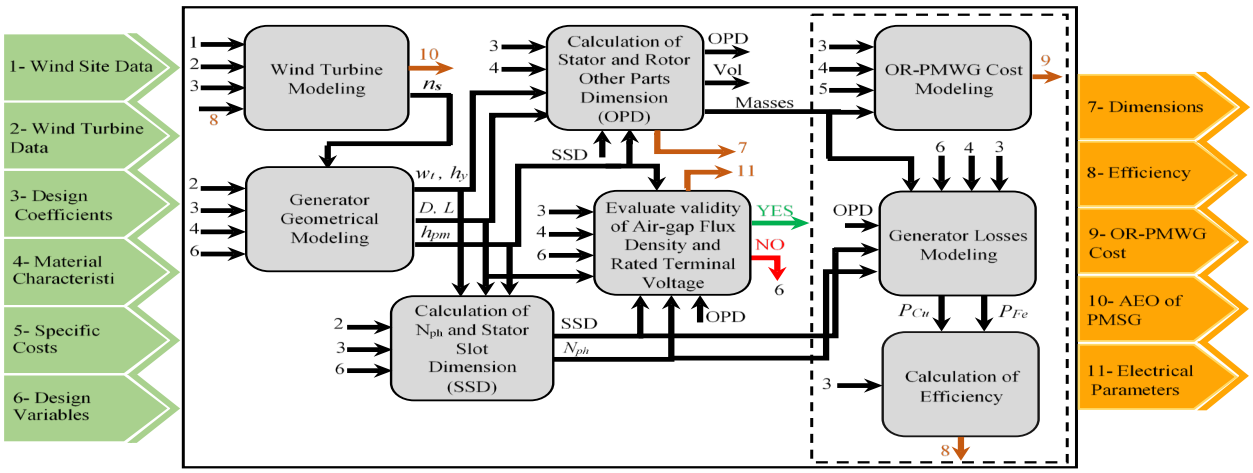

Figure 6. Design flowchart of the OR-OMWG

3. The design variables

In order to obtain an optimal design, the design variables are determined first. Then, their impacts on the GSC and AEO are investigated. The design variables are presented in Table 3. Two effective parameters within the optimal design process are Am and Bmg and their impact alongside the other parameters are shown in Figures 7 and 8.

Table 3. The design variables and their boundaries

Design variables	Range	
	Min	Max
A_m (kA/m)	10	55
B_{mg} (T)	0.738	0.984
L/D	0.14	0.5
ϵ	1	1.4
α_i	0.6	0.9
P	8	64
B_y Stator (T)	1.1	1.5
B_y Rotor (T)	1.3	1.6
B_t (T)	1.5	2

To provide a better visual representation of the impact of the design variables, the GSC and AEO are shown in Figure 7 in separate 3D subplots, while the A_m and another effective parameter are considered as two variables. It can be seen from Figure 7a that maximum AEO can be achieved when A_m varies between 20 and 30 kA/m and B_{mg} ranges between 0.8 and 0.9 T. Moreover, Figure 7b shows that the lowest GSC occurs at A_m and B_{mg}. According to Figure 7c, when A_m varies between 20 and 40 kA/m and the pole-arc to pole-pitch ratio α_i is in the range of 0.8 to 0.9, the maximum AEO is delivered. According to Figure 7d, the generation system cost is minimum when α_i=0.6 and A_m=60 kA/m. Figure 7e shows that when A_m and L/D ratio ranges between 30-50 kA/m and 0.14-0.2, respectively, the AEO can be maximum. According to Figure 7f, the lowest cost is obtained when L/D=0.14 and A_m=60 kA/m. The impacts of A_m and pole number P on GSC and AEO are investigated, as shown in Figures 7g and 7h, respectively. The lowest generation system cost is achieved when A_m varies between 20 and 30 kA/m and the pole number is 20. Moreover, minimum GSC is related to A_m and maximum pole number is found in Figure 7h. Figure 7i shows that the maximum AEO is restricted to A_m in the range of 20 to 30 kA/m, while the ratio of induced voltage to full load terminal voltage ϵ is minimum. According to Figure 7j, the minimum cost is computed when ϵ =1 and A_m=60 kA/m. Furthermore, according to Figure 7k, maximum AEO belongs to the area with A_m at about 25 kA/m, while the peak tooth flux density B_t varies from 1.6 to 1.75 T. As shown in Figure 7l, minimum GSC occurs at A_m and B_t does not have a significant effect on it.

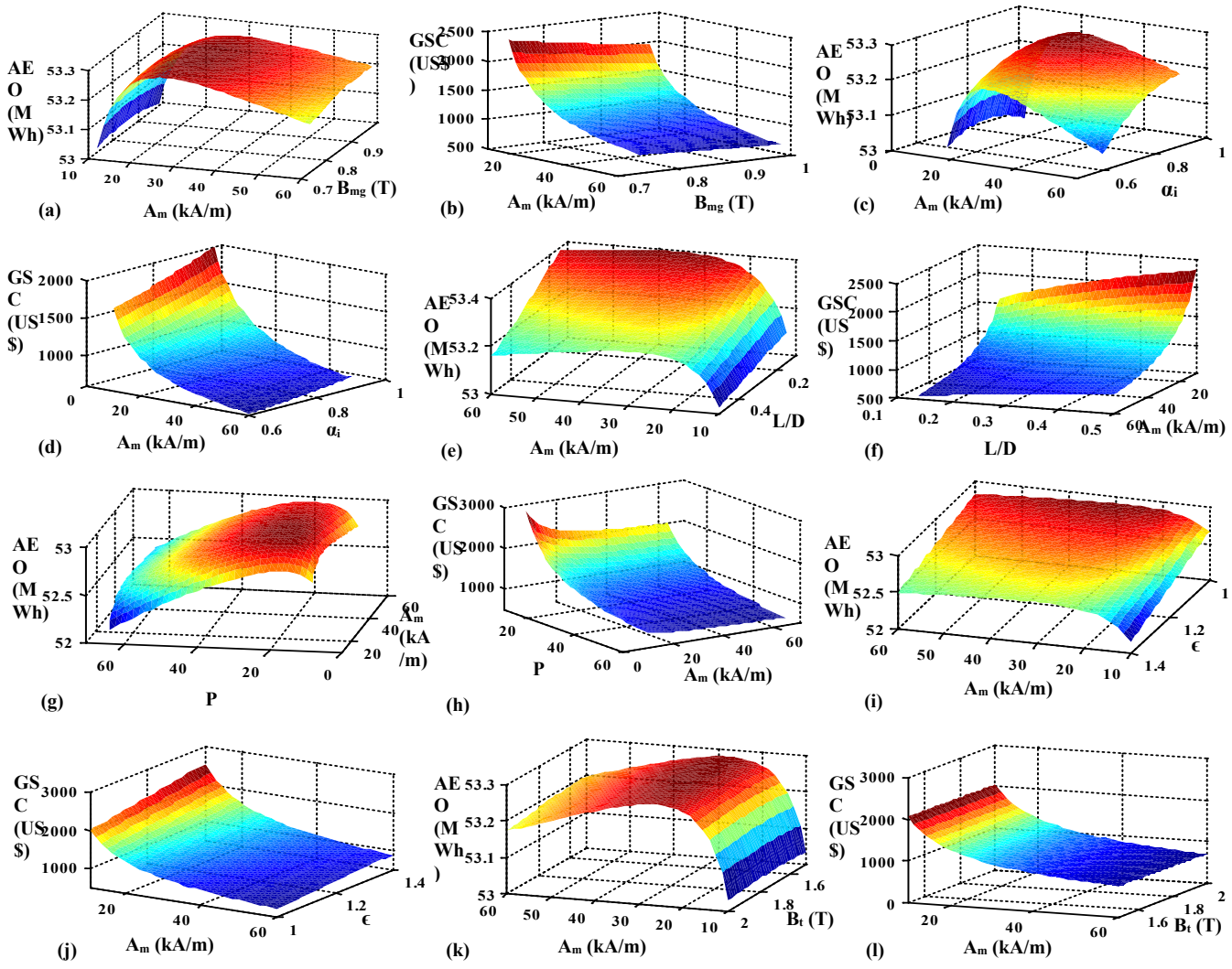

Figure 7. Impacts of A_m and other design variables on GSC and AEO

Similarly, in Figure 8, the impact of maximum air gap flux density and other optimization variables on the generation system cost and AEO is shown. It is clearly observed from Figure 8a that the maximum AEO is obtained when α_i is in the range of 0.75-0.85 and B_{mg}=0.984 T. According to Figure 8b, the minimum GSC value is computed when B_{mg}=0.738 T and α_i=0.9. The impact of B_{mg} and the ratio of L/D on AEO are depicted in Figure 8c where its maximum values are available where L/D varies between 0.35 and 0.45 and B_{mg}=0.738 T. Figure 8d shows that the lowest GSC occurs at B_{mg}=0.738 T and L/D =0.5. In Figures 8e and 8f, the impact of B_{mg} and pole number on GSC and AEO is investigated. The maximum P as well as the maximum value of B_{mg} result in the minimum generation system cost. Besides, the maximum AEO is obtained when pole number is 20 and B_{mg}=0.984 T. It is seen in Figure 8g that when B_{mg} ranges between 0.85 and 0.95 T and ϵ=1, the maximum AEO is obtained. According to Figure 8h, the minimum GSC belongs to B_{mg}=0.984 T and ϵ=1. The impact of B_t and B_{mg} on AEO is shown in Figure 8i. It is observed that the maximum AEO is when B_{mg} and B_t are in the range of 0.8-0.85 T and 1.85-1.95 T, respectively. Also, as depicted in Figure 8j, the minimum generation system cost is observed at B_{mg}=0.984 T and B_t=2 T.

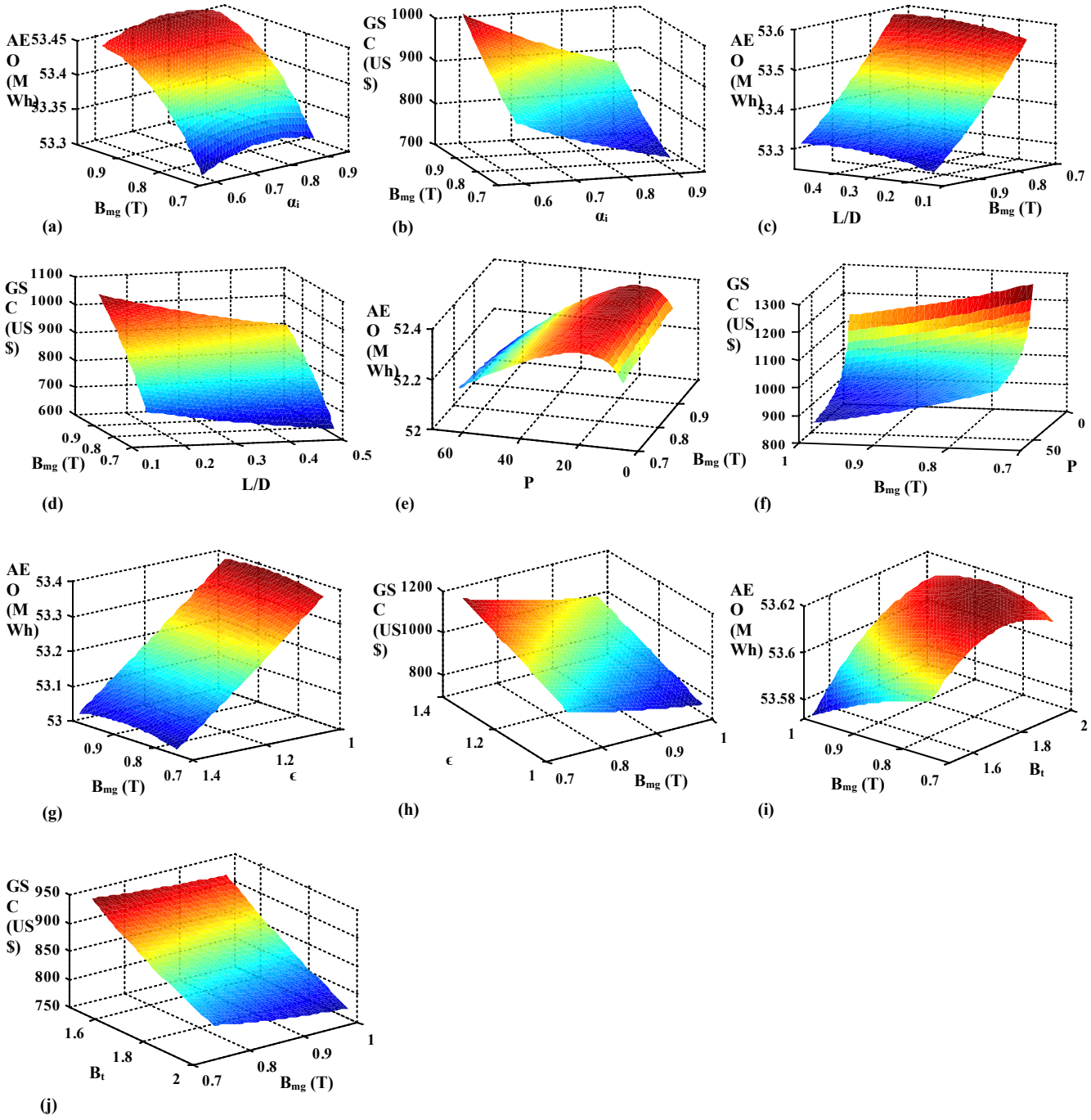

Figure 8. Impacts of B_{mg} and other design variables on GSC and AEO

4. Design optimization and results

The aim of this paper is to make a viable agreement between the cost and the AEO of generation system. In fact, the optimization procedure is considered in two parts, single-objective and multi-objective methods. In the case of single-objective method, the OR-PMWG cost and the AEO of

generation system are optimized separately. In the multi-objective method, these requirements are optimized simultaneously. The Lower Boundaries (LB) and the Upper Boundaries (UB) of design variables are listed in Table 3. To this point, three optimization cases have been employed:

Case A: The objective minimizes the OR-PMWG cost using Eq. (26).

Case B: The objective maximizes the AEO of generation system using Eq. (27).

Case C: The objective is used to optimize the multi-objective function given by Eq. (28).

$$F_1 = C_t \tag{26}$$

$$F_2 = \frac{1}{AEO_G} \tag{27}$$

$$F_3 = \frac{AEO_{G,ref}}{AEO_G} + \frac{C_t}{C_{t,ref}} \tag{28}$$

where $C_{t,ref}$ is the minimum value of the OR-PMWG cost and $AEO_{G,ref}$ is the maximum value of the AEO of generation system, which will be obtained by optimizing F_1 and F_2, respectively. Optimization results of different objective functions are listed in Table 4. It can be observed that Case B is more expensive, but gives more energy (AEO_G) than Case A. In comparison to Case A, Case B presents the increase of US$2096.44 (84.57 %) in the OR-PMWG cost corresponding to an increase in the AEO_G of 2.52 MWh (3.56 %). Consequently, Case A is a poor choice in terms of AEO of generation system, and the Case B is a poor choice in terms of manufacturing cost. It is clear that any attempt to achieve a high AEO for the generation system or a low OR-PMWG cost deteriorates other requirement. Therefore, a multi-objective optimization is required to make a satisfactory compromise between the OR-PMWG cost and the AEO of generation system. To this end, a flexible multi-objective function is defined as Eq. (28). According to Table 4, it is seen that compared to Case B, Case C (C_t= US$2651.51) presents a considerable reduction in the OR-PMWG cost and a moderate reduction in the AEO of the generation system. Also, compared to Case A, the AEO_G of Case C is 657.75 kWh higher with the moderate increase of US$172.53 (6.96 %) in the OR-PMWG cost. Thus, it yields a good compromise between the OR-PMWG cost and AEO of the generation system. The improvement of the multi-objective function F_3 in iterations of the optimization process is shown in Figure 9. Finally, the probability function of the Rayleigh distribution at an average wind speed of 8.7 m/s is seen in Figure 10a and the annual energy output of the generation system as a function of discrete wind speed is shown in Figure 10b.

Table 4. The optimization results for different objectives

Parameters	Range		The optimized values for different objectives		
	LB	UB	Case A	Case C	Case B
Am (kA/m)	10	55	47.86	36.21	11.93
Bmg (T)	0.738	0.984	0.982	0.983	0.981
L/D	0.14	0.5	0.16	0.17	0.21
ϵ	1	1.4	1.33	1.15	1.09
αi	0.6	0.9	0.77	0.83	0.88
P	8	64	12	12	14
By Stator (T)	1.1	1.5	1.49	1.35	1.1
By Rotor (T)	1.3	1.6	1.59	1.59	1.42
Bt (T)	1.5	2	1.55	1.51	1.75
AEOG (MWh)			70.73	71.39	73.25
OR-PMWG cost (US$)			2478.98	2651.51	4575.42
Generator full-load efficiency (%)			94.01	95.11	96.27
Generator full-load total losses (W)			955.45	771.01	579.94
g (mm)			0.56	0.58	0.73
f			15	15	17.5
Line-to-line Erms (V)			546.25	463.3	445.22

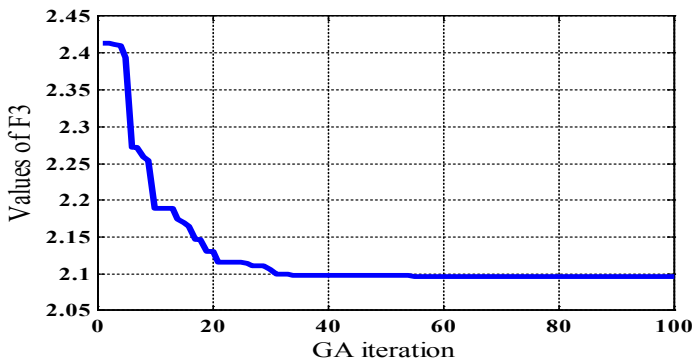

Figure 9. The improved values of F3 for the first 100 iterations

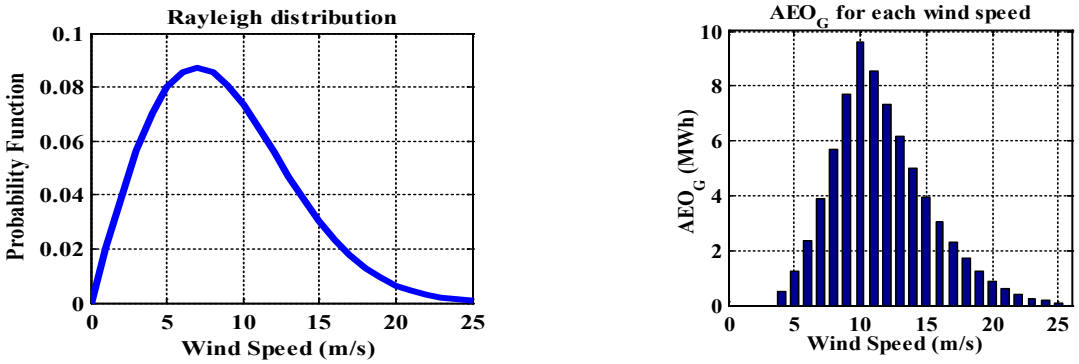

(a) (b)

Figure 10. (a) Rayleigh distribution at an average wind speed of 8/7 m/s, (b) AEO of the generation system as a function of discrete wind speed

4.1. Comparison with prototype generator

As shown in Table 5, the optimized generator parameters are presented and compared with a three-phase 15 kW direct-drive outer rotor permanent magnet wind power generator prototype, which was built and tested. It was found that the proposed optimization design achieved lower total volume and higher efficiency. On the other hand, the optimized generator is characterized by a six-phase configuration, which make it superior to the three-phase prototype generator in terms of reliability.

Table 5. Comparison of the optimized generator and prototype generator characteristics

Design parameters	OR-PMSG optimized parameters	PM generator grototype parameters [17]
Total volume (cm^3)	33094.1	33541.39
Efficiency	95.11	94.4
Stator outer diameter (D) (mm)	581.41	623
Generator outer diameter (D_e) (mm)	650.63	653.5
Magnet thickness (mm)	3.33	6
Stator stack length (mm)	99.54	100
Nominal line voltage (V)	408	408
Magnet to pole pitch ratio (α_i)	0.83	0.73
Frequency (Hz)	15	50
Number of poles	12	40
Nominal rotational speed (rpm)	150	150

5. FEA verification

In this section, the 3D FEA simulation method is used for verifying the effectiveness of the analytical design procedure (ADP) presented in this study. To do this, the Ansoft-MAXWELL® v.16 software package is employed. In the generator simulation process, resistive load is used because of a unitary PF considered in the design model. The evaluation is performed by a comparison of the optimized generator parameters and the FEA results, which can be seen in Table 6. It is observed that the difference between the ADP and FEA results is less than 2 %. Figure 11a depicts the mesh diagram of the generator finite element model, and Figure 11b shows the flux density distribution in various parts of the machine.

Table 6. Comparison between ADP and FEM results

PMSG parameters	ADP results	FEA results	Error (%)
Line-to-line E_{rms} (V)	463.3	461.7	0.34
V_L (V)	400	398.3	0.42
B_{mg1} (T)	1.21	1.19	1.65
P_{out} (W)	15000	14965	0.23
P_{in} (W)	15771	15748	0.14
B_y Stator (T)	1.35	1.33	1.5
B_y Rotor (T)	1.59	1.56	1.9
B_t (T)	1.51	1.5	0.66

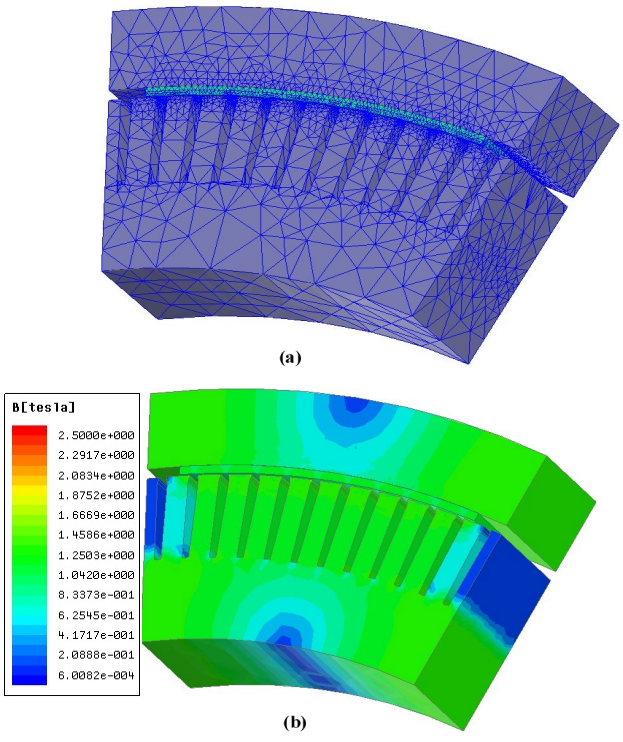

Figure 11. (a) The finite element mesh of the generator, (b) The magnetic flux density distribution of the generator

The curve of magnetic air gap flux density distribution is shown by Figure 12a under no-load conditions, in which the fundamental air gap flux density highest value (B_{mg1}) is measured 1.19 (T). Figure 12b shows the line-induced voltage waveforms in the no-load condition (line-to-line E_{rms}). The fundamental rms value E_{rms} is computed 461.7 (V) and the total harmonic distortion (THD) of voltage is 4.21 %. The waveforms of full-load terminal line voltages (V_L) are shown in Figure 12c. Fundamental rms value of these voltages is 398.3 V and their THD = 0.72 %. The waveform of the output power (P_{out}) in the full-load condition is given in Figure 12d. Its average value in steady state conditions is measured at about 14965 (W). Figure 12e shows the input power (P_{in}) waveform of the generator in the full-load condition. The average value of the measured input power is about 15748 W in steady-state conditions.

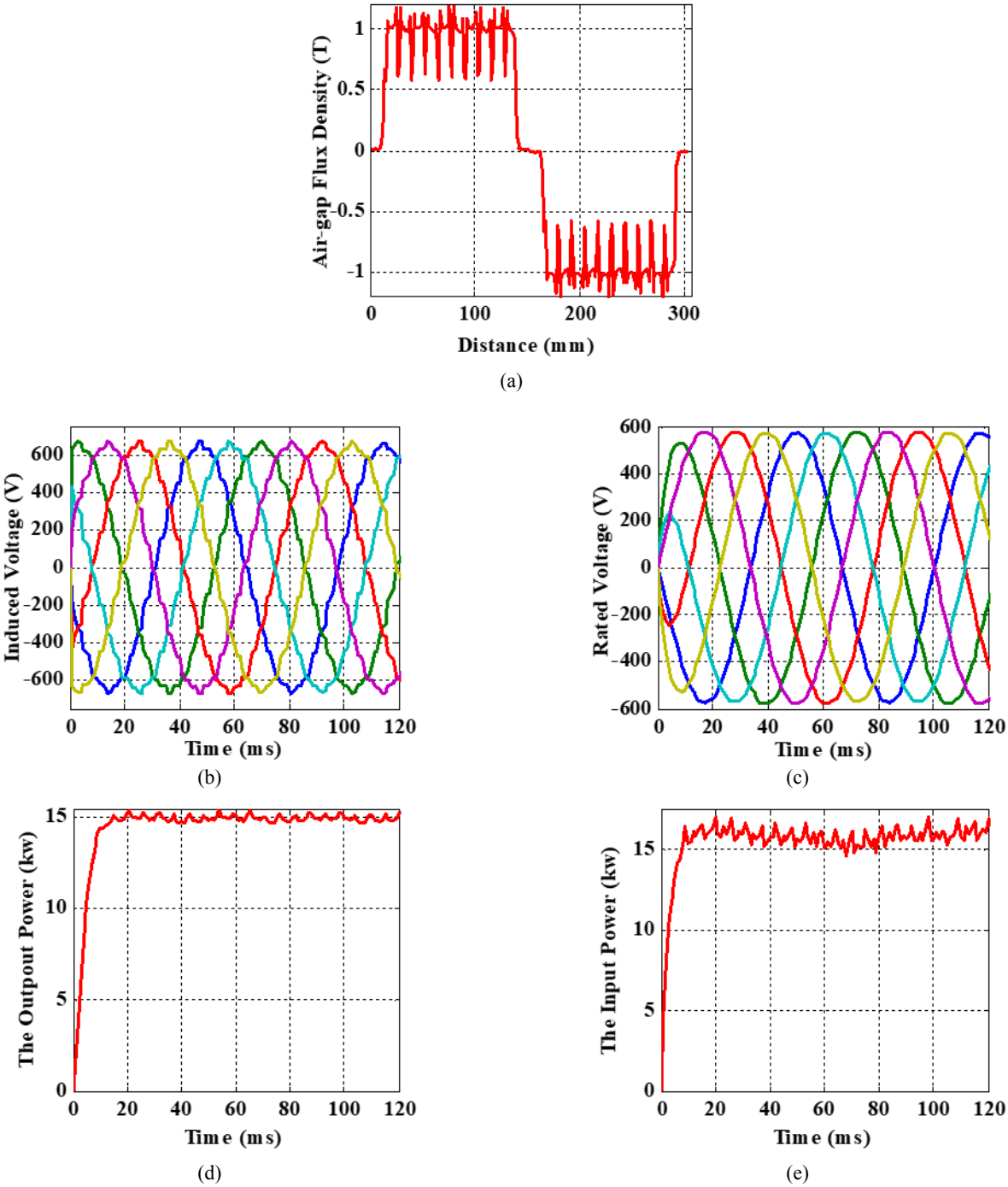

Figur 12. (a) Air-gap flux density curve, (b) No-load terminal line voltages, (c) Nominal line voltages, (d) The waveform of the generator full-load output power, (e) The waveform of the generator input power in the full-load condition

6. CONCLUSIONS

This study made an attempt to establish a multi-objective optimal design for a small-scale direct-drive wind power system in accordance with a PM synchronous generator with outer-rotor. This optimization problem was aimed at obtaining an optimum cost-effective OR-PMWG, i.e., high AEO and low cost of generation systems. The presented accurate model and design flowchart of OR-PMWG were the main novelties of this paper. In this regard, the generation system was firstly optimized for each of the objectives independently. Then, a multi-objective optimization design considering all the objectives was provided. It was also demonstrated that the

proposed multi-objective optimization afforded reliable performance in view of OR-PMWG design. It was shown that the AEOG was 657.75 (KWh) higher and GSC was 1923.91 (US$) lower than single-objective functions. To this end, the GA was applied to handling the optimization process. Furthermore, a comparison was made between the influential characteristics of the optimized generator and a prototype outer-rotor PM generator, indicating that the performance of the optimized PMSG was superior to that of the prototype generator in terms of efficiency as well as total volume. Moreover, as demonstrated by the results, the six-phase OR-PMWG was found to be more reliable. Eventually, the three-dimensional Finite Element Analysis (FEA) justifies the results obtained from the numerical optimization.

7. ACKNOWLEDGEMENT

The authors gratefully acknowledge the funding support obtained from Babol Noshirvani University of Technology with grant program numbers BNUT/370509/00 and BNUT/390066/00.

REFERENCES

1. Eterafi, S., Gorjian, S. and Amidpour, M., "Effect of covering aperture of conical cavity receiver on thermal performance of parabolic dish collector: Experimental and numerical investigations", ***Journal of Renewable Energy and Environment (JREE)***, Vol. 8, No. 4, (2021), 29-41. (https://dx.doi.org/10.30501/jree.2021.275871.1194).
2. Hosseini, E., Behzadfar, N., Hashemi, M., Moazzami, M. and Dehghani, M., "Control of pitch angle in wind turbine based on doubly fed induction generator using fuzzy logic method", ***Journal of Renewable Energy and Environment (JREE)***, Vol. 9, No. 2, (2022), 1-7. (https://dx.doi.org/10.30501/jree.2021.293546.1226).
3. Global Wind Energy Council, "Global wind report: Annual market update 2021", (2021). (https://gwec.net/wp-content/uploads/2021/03/GWEC-Global-Wind-Report-2021.pdf), (Accessed: 11 March 2021).
4. Jahangiri, M., Karimi Shahmarvandi, F. and Alayi, R., "Renewable energy-based systems on a residential scale in southern coastal areas of Iran: Trigeneration of heat, power, and hydrogen", ***Journal of Renewable Energy and Environment (JREE)***, Vol. 8, No. 4, (2021), 67-76. (https://dx.doi.org/10.30501/jree.2021.261980.1170).
5. Abdoos, A.A., Moazzen, M.E. and Hosseini, S.M., "Optimal design of an exterior-rotor permanent magnet generator for wind power applications", ***Journal of Operation and Automation in Power Engineering (JOAPE)***, Vol. 9, No. 3, (2021), 193-202. (https://doi.org/10.22098/JOAPE.2021.7337.1532).
6. Grauers, A., "Design of direct-driven permanent-magnet generators for wind turbines", Doctoral Thesis at School of Electrical and Computer Engineering, Chalmers University of Technology, (1996), 76-79. (https://www.osti.gov/etdeweb/servlets/purl/442505).
7. Hailemariam, Z.M., Leidhold, R. and Tesfamariam, G.T., "Real-time dc-link voltage control of 5-kW PMSG-based wind turbine generator through a test-rig", ***Electrical Engineering (EE)***, Vol. 103, (2021), 1869-1880. (https://doi.org/10.1007/s00202-020-01176-3).
8. Polinder, H., Pijl, F., Vilder, G. and Tavner, P., "Comparison of direct-drive and geared generator concepts for wind turbines", ***IEEE Transactions on Energy Conversion (IEEETEC)***, Vol. 23, No. 3, 725-733, (2006). (https://doi.org/10.1109/TEC.2006.875476).
9. Puri, V., Chauhan, Y.K. and Singh, N., "A comparative design study and analysis of inner and outer rotor permanent magnet synchronous machine for power generation in vertical axis wind turbine using GSA and GSA-PSO", ***Sustainable Energy Technologies and Assessments (SETA)***, Vol. 23, (2017), 136-148. (https://doi.org/10.1016/j.seta.2017.09.008).
10. Tapia, J., Pyrhönen, J., Puranen, J., Lindh, P. and Nyman, S., "Optimal design of large permanent magnet synchronous generators", ***IEEE Transactions on Magnetics (IEEETM)***, Vol. 49, No. 1, (2013), 642-650. (https://doi.org/10.1109/TMAG.2012.2207907).
11. Chen, J., Nayar, C.V. and Xu, L., "Design and finite-element analysis of an outer-rotor permanent-magnet generator for directly coupled wind turbines", ***IEEE Transactions on Magnetics (IEEETM)***, Vol. 36, No. 5, (2000), 3802-3809. (https://doi.org/10.1109/20.908378).
12. Li, H., Chen, Z. and Polinder, H., "Optimization of multibrid permanent- magnet wind generator systems", ***IEEE Transactions on Energy Conversion (IEEETEC)***, Vol. 24, No. 1, (2009), 82-92. (https://doi.org/10.1109/TEC.2008.2005279).
13. Lee, S., Kim, Y., Lee, K. and Kim, S., "Multiobjective optimization design of small-scale wind power generator with outer-rotor based on box–behnken design", ***IEEE Transactions on Applied Superconductivity (IEEETASC)***, Vol. 26, No. 4, (2016), 605-609. (https://doi.org/10.1109/TASC.2016.2524620).
14. Bazzo, T.P.M., Kolzer, J.F., Carlson, R., Wurtz, F. and Gerbaud, L., "Multiphysics design optimization of a permanent magnet synchronous generator", ***IEEE Transactions on Industrial Electronics (IEEETIE)***, Vol. 64, No. 12, (2017), 9815-9823. (https://doi.org/10.1109/TIE.2017.2726983).
15. McDonald, A. and Bhuiyan, N., "On the optimization of generators for offshore direct drive wind turbines", ***IEEE Transactions on Energy Conversion (IEEETEC)***, Vol. 32, No. 1, (2017), 348-358. (https://doi.org/10.1109/TEC.2016.2624219).
16. Asef, P., Perpiñà, R.B., Barzegaran, M.R., Lapthorn, A. and Mewes, D., "Multiobjective design optimization using dual-level response surface methodology and booth's algorithm for permanent magnet synchronous generators", ***IEEE Transactions on Energy Conversion (IEEETEC)***, Vol. 33, No. 2, (2018), 652-659. (https://doi.org/10.1109/TEC.2017.2777397).
17. Potgieter, J.H.J. and Kamper, M.J., "Torque and voltage quality in design optimization of low-cost non-overlap single layer winding permanent magnet wind generator", ***IEEE Transactions on Industrial Electronics (IEEETIE)***, Vol. 59, No. 5, (2012), 2147-2156. (https://doi.org/10.1109/TIE.2011.2159955).
18. Öztürk, N., Dalcalı, A., Çelik, E. and Sakar, S., "Cogging torque reduction by optimal design of PM synchronous generator for wind turbines", ***International Journal of Hydrogen Energy (IJHE)***, Vol. 42, (2017), 17593-17600. (https://doi.org/10.1016/j.ijhydene.2017.02.093).
19. Sedaghat, A., El Haj Assad, M. and Gaith, M., "Aerodynamics performance of continuously variable speed horizontal axis wind turbine with optimal blades", ***Energy***, Vol. 77, (2014), 752-759. (https://doi.org/10.1016/j.energy.2014.09.048).
20. Sedaghat, A., Samani, I., Ahmadi-Baloutaki, M., El Haj Assad, M. and Gaith, M., "Computational study on novel circulating aerofoils for use in Magnus wind turbine blades", ***Energy***, Vol. 91, (2015), 393-403. (https://doi.org/10.1016/j.energy.2015.08.058).
21. Abidoye, L.K., Bani-Hani, E., El Haj Assad, M., AlShabi, M., Soudan, B. and T Oriaje, A., "Effects of environmental and turbine parameters on energy gains from wind farm system: Artificial neural network simulations", ***Wind Engineering (WE)***, Vol. 44. No. 2, (2019), 181-195. (https://doi.org/10.1177/0309524X19849834).
22. Bazzo, T.P.M., Kolzer, J.F., Carlson, R., Wurtz, F. and Gerbaud, L., "Multidisciplinary design optimization of direct-drive PMSG considering the site wind profile", ***Electric Power Systems Research (EPSR)***, Vol. 141, (2016), 467-475. (http://dx.doi.org/10.1016/j.epsr.2016.08.023).
23. Li, F. and Zhu, X., "Comparative study of stepwise optimization and global optimization on a nine-phase flux-switching PM generator", ***Energies***, Vol. 14, No. 16, (2021), 4754. (https://doi.org/10.3390/en14164754).
24. Singh, G., Kumar, A. and Saini, R., "Performance evaluation of series compensated self-excited six-phase induction generator for stand-alone renewable energy generation", ***Energy***, Vol. 35, No. 1, (2010), 288-297. (https://doi.org/10.1016/j.energy.2009.09.021).
25. Pyrhönen, J., Jokinen, T. and Hrabovcová, V., Design of rotating electrical machines, Wiley, USA, (2009), 512-519. (https://doi.org/10.1002/9781118701591).
26. Boldea, I., Variable speed generators, CRC Press, (2005), 420-423. (https://doi.org/10.1201/b19293).
27. Gieras, J.F., Permanent magnet motor technology, design and applications, CRC Press, (2010), 100-102. (https://doi.org/10.1201/9780429292736).
28. Kurt, E, Gör, H. and Çelik, K., "Optimization of a 3-kW axial flux permanent magnet generator with variable air gap", ***International***

Transactions on Electrical Energy Systems (ITEES), Vol. 31, No. 11, (2021), e13074. (https://doi.org/10.1002/2050-7038.13074).

29. Khan, A. and Pillay, P., "Design of a PM wind, optimized for energy capture over a wide operating range", ***IEEE International Conference on Electrical Machines and Drives***, San Antonio, TX, USA, (2005), 1501-1506. (https://doi.org/10.1109/IEMDC.2005.195919)
30. Wang, T. and Wang, Q., "Optimization design of a permanent magnet synchronous generator for a potential energy recovery system", ***IEEE Transactions on Energy Conversion (IEEETEC)***, Vol. 27, No. 4, (2012), 856-863. (https://doi.org/10.1109/TEC.2012.2211080).
31. Eriksson, S. and Bernhoff, B., "Loss evaluation and design optimization for direct driven permanent magnet synchronous generators for wind power", ***Applied Energy (AE)***, Vol. 88, No. 1, (2011), 265-271. (https://doi.org/10.1016/j.apenergy.2010.06.010).
32. Jagau, H., Khan, M.A. and Barendse, P., "Design of a sustainable wind generator system using redundant material", ***IEEE Transactions on Industry Applications (IEEETIA)***, Vol. 23, No. 6, (2012), 1827-1837. (https://doi.org/10.1109/TIA.2012.2221672).
33. Iranian Renewable Energy Organization Magazine, (2010). (In Farsi). (http://www.satba.gov.ir/suna_content/media/image/2015/11/4222_orig.pdf), (Accessed: 15 July 2010).
34. Abdoos, A.A., Moazzen, M.E. and Ebadi, A., "Optimal design of a radial-flux permanent magnet generator with outer-rotor for direct-drive wind turbines", ***Computational Intelligence in Electrical Engineering (CIEE)***, Vol. 11, No. 4, (2020), 51-64. (In Farsi). (https://dx.doi.org/10.22108/isee.2020.117057.1227).